

Chalmers Publication Library



CHALMERS

Copyright Notice IEEE

©2013 IEEE. Personal use of this material is permitted. However, permission to reprint/republish this material for advertising or promotional purposes or for creating new collective works for resale or redistribution to servers or lists, or to reuse any copyrighted component of this work in other works must be obtained from the IEEE.

(Article begins on next page)

— *b) Variation of the numbers of cylinders (n).*

As expected, the higher the number of cylinders considered, the greater the multiple-diffraction attenuation obtained. The influence of the variation of the parameter n is more significant at negative angles of incidence, where a greater difference is observed between $n = 1$ and $n = 3$ (maximum difference of 8.5 dB) than between $n = 3$ and $n = 5$ (maximum difference of 4 dB).

— *c) Variation of the distance between the transmitter and the series of cylinders (d).*

As mentioned in the previous section, because parameter H was considered from -0.02 m to 0.02 m when $d = 0.20$ m, and from -0.01 m to 0.01 m for $d = 0.10$ m, the incident angle α had the same maximum value of 5.2° (and -5.2° for $H < 0$) for the two considered values of the distance between the transmitter and the cylinders. However, the curves corresponding to the different values of d , when assuming the same n , r , and polarization, are not identical, due to the fact that although the same range of angles of incidence is evaluated, the wave front is considered to be spherical and therefore, the attenuation obtained in every case is different because the distance covered by the wave is not the same. Thus, there exists more attenuation at a given negative angle of incidence for $d = 0.20$ m (a maximum difference of 1.37 dB for $\alpha = -5.2^\circ$, $n = 5$, $r = 0.02$ m, and *hard/vertical* polarization), but the opposite occurs for positive values of α , where the value $d = 0.10$ m shows more losses due to multiple diffraction (a maximum difference of 3.29 dB for $\alpha = 5.2^\circ$, $n = 5$, $r = 0.02$ m, and *hard/vertical* polarization).

— *d) Variation of the type of polarization.*

The influence of the type of polarization is more relevant at negative angles of incidence, where the *soft/horizontal* polarization results show a greater attenuation with respect to the *hard/vertical* polarization case (up to 7 dB of difference).

V. CONCLUSIONS

A UTD-PO solution for the analysis of multiple-cylinder diffraction has been validated through measurements performed at 60 GHz. A parametric study has been carried out both theoretically and experimentally in which the influence of: the number of cylinders, the radius of curvature, the distance from the transmitter to the array of rounded surfaces, and the polarization has been analyzed. The solid agreement found between the predicted and measured results (with a Mean Error ranging from 0.12 to 0.71 dB) shows that the UTD-PO theoretical formulation can be applied for radiowave propagation studies when multiple-diffraction over cylindrical surfaces has to be taken into account.

REFERENCES

- [1] H. H. Xia and H. L. Bertoni, "Diffraction of cylindrical and plane waves by an array of absorbing half-screens," *IEEE Trans. Antennas Propag.*, vol. 40, no. 2, pp. 170–177, 1992.
- [2] W. Zhang, "A more rigorous UTD-based expression for multiple diffractions by buildings," *IEE Proc. Microw. Antennas Propag.*, vol. 142, no. 6, pp. 481–484, 1995.
- [3] A. Kara and E. Yazgan, "Roof shape modelling for multiple diffraction loss in cellular mobile communication systems," *Int. J. Electron.*, vol. 89, no. 10, pp. 753–758, 2002.
- [4] L. Juan-Llácer and J. L. Rodríguez, "A UTD-PO solution for diffraction of plane waves by an array of perfectly conducting wedges," *IEEE Trans. Antennas Propag.*, vol. 50, no. 9, pp. 1207–1211, 2002.
- [5] D. Erricolo and P. L. E. Uslenghi, "Two-dimensional simulator for propagation in urban environments," *IEEE Trans. Veh. Technol.*, vol. 50, no. 4, pp. 1158–1168, 2001.
- [6] R. Janaswamy and J. B. Andersen, "Path loss predictions in urban areas with irregular terrain topography," *Wireless Personal Commun.*, vol. 12, pp. 255–268, 2000.

- [7] G. Koutitas and C. Tzaras, "A UTD solution for multiple rounded surfaces," *IEEE Trans. Antennas Propag.*, vol. 54, no. 4, pp. 1277–1283, Apr. 2006.
- [8] J.-V. Rodríguez, J.-M. Molina-García-Pardo, and L. Juan-Llácer, "A hybrid UTD-PO solution for multiple-cylinder diffraction analysis assuming spherical-wave incidence," *IEEE Trans. Antennas Propag.*, vol. 56, no. 9, pp. 3078–3081, Sep. 2008.
- [9] M.-T. Martínez-Inglés, C. García-Pardo, J. Pascual-García, J.-M. Molina-García-Pardo, J.-V. Rodríguez, J. Reig, and L. Juan-Llácer, "Initial experimental characterization of the millimeter-wave radio channel," presented at the Eur. Conf. on Antennas and Propagation, Prague, Czech Republic, Mar. 23–30, 2012.
- [10] J.-M. Molina-García-Pardo, J.-V. Rodríguez, and L. Juan-Llácer, "Wide-band measurements and characterization at 2.1 GHz while entering in a small tunnel," *IEEE Trans. Veh. Technol.*, vol. 53, no. 6, pp. 1794–1799, Nov. 2004.
- [11] J.-V. Rodríguez, J.-M. Molina-García-Pardo, and L. Juan-Llácer, "A new solution expressed in terms of UTD coefficients for the multiple diffraction of spherical waves by a series of buildings," *Radio Sci.*, vol. 42, p. RS4011, 2007, 10.1029/2006RS003464.

Characterization of Implemented Algorithm for MIMO Spatial Multiplexing in Reverberation Chamber

Xiaoming Chen, Per-Simon Kildal, and Mattias Gustafsson

Abstract—Previously, the throughput for a single-input multiple-output (SIMO) system was successfully tested in a reverberation chamber (RC), and the results were in good agreement with a model based on the ideal threshold receiver. In the present communication, we measure the throughput of a 2×2 open loop multiple-input multiple-output (MIMO) system with full spatial multiplexing (i.e., two data streams), and we compare the results with an extended throughput model taking the spatial multiplexing into account. The measured throughput is found to be in agreement with the simulated one of a simple zero-forcing (ZF) receiver. The throughput degradations due to correlation and power imbalance (caused by different embedded radiation efficiencies of antennas) are studied and referred to as a throughput multiplexing efficiency. These can, to a large extent, be explained by the ZF algorithm. The results show clearly that the rich isotropic multipath (RIMP) environment generated by an RC can be used to study how effective different MIMO algorithms are when there is correlation and efficiency imbalance between the antenna elements.

Index Terms—Multiple-input multiple-output (MIMO), reverberation chamber, rich isotropic multipath, throughput.

I. INTRODUCTION

Reverberation chambers (RCs) have been successfully used in various over-the-air (OTA) [1]–[7] tests of wireless devices due to its rich isotropic multipath (RIMP) characteristics [8]. The RC can be used to measure bit error rate (BER) of a communication system [1], [2] as well as the radiated power and the receiver sensitivity of mobile terminals

Manuscript received March 18, 2013; revised April 07, 2013; accepted April 16, 2013. Date of publication April 23, 2013; date of current version July 31, 2013. This work was supported in part by the cooperation project "uBTS HO-MIMO antenna" funded by Huawei Technologies.

X. Chen and P.-S. Kildal are with the department of Signals and Systems, Chalmers University of Technology, Gothenburg, Sweden (e-mail: xiaoming.chen@chalmers.se).

M. Gustafsson is with Huawei Technologies Sweden AB, Gothenburg, Sweden.

Color versions of one or more of the figures in this communication are available online at <http://ieeexplore.ieee.org>.

Digital Object Identifier 10.1109/TAP.2013.2259459

[3]. Very recently, the RC has been used to measure the throughput of a WLNA (wireless local network) system [5] and a LTE (long term evolution) system [6]. A throughput model was developed in [6] that could be used to predict the measured throughput with the absolute value of the required power level in the order of fractions of one dB. Nevertheless, the work in [6] was limited to a single-input multiple-output (SIMO) LTE system. Namely, the model in [6] takes the antenna diversity and the orthogonal frequency division multiplexing (OFDM) into account, but not the spatial multiplexing, which is probably the most important feature of a MIMO system.

In this communication, we extend the throughput model to a multi-input multiple-output (MIMO) system, accounting for both OFDM and spatial multiplexing. The MIMO throughput was previously studied in [7] with a model that accurately predicted the conductive measurements, but not correctly accounting for multiplexing algorithms in the fading case. In the present communication we try to understand the effects power imbalance and correlation on throughput by using a zero-forcing (ZF) receiver. A multiplexing efficiency is used to describe the degradations due to power imbalance and correlation.

II. THROUGHPUT MODEL

The goal of modeling the throughput of a MIMO system is to complement the RC measurements and to provide insight into the OTA testing of LTE devices. A throughput model for a MIMO-OFDM system was presented in [10]. However, the model in [10] can only be used to predict uncoded BER performances and the advanced error-correcting code in the LTE system is not included in the model. A simple way to include the advanced coding of a LTE system is to use the threshold receiver model [6]. The threshold model works for systems with advanced coding. We assume that the threshold receiver ideally can correct for bit errors so that the package error rate, or group error rate (GER) [6], jumps from 100% to 0% at a certain threshold of the received power. Mathematically, the GER of an ideal threshold receiver in an AWGN¹ channel can be expressed as

$$GER_{ideal}(P_0) = \begin{cases} 1, & P_0 < P_t \\ 0, & P_0 > P_t \end{cases} \quad (1)$$

where P_0 is the received power in the AWGN channel, P_t is the threshold value. It has been shown in [6] that, in the RIMP environment of a well-stirred RC, the throughput of the threshold receiver becomes

$$T(P) = T_{\max} CCDF \left(\frac{P_t}{P} \right) \quad (2)$$

where T_{\max} is the maximum achievable throughput, $CCDF$ stands for complementary cumulative distribution function (CDF), and P is the average received power in the fading environment. Note that we define the relative throughput as T/T_{\max} , and we will use this hereafter.

Interestingly, the threshold receiver model can be justified by the outage theorems [11]. It has been proved in [11] that with powerful hybrid-automatic-repeat-request coding the GER in a fading environment can be well approximated by the outage probability of the fading channel.

Based on (2), the throughput in a fading environment can be readily calculated once the CDF of the received power is known. The absolute power calibration is done using the threshold power level P_t (that can be measured conductively) and the average power transfer function in the RC. In [6], the receiver in a SIMO LTE system was modeled by using the maximum ratio combining (MRC) algorithm. In the present work, we deal with the more advanced spatial multiplexing case. In order to use the throughput model (2), we need to calculate the CDF

¹An AWGN channel is a channel with constant signal (no fading) and additive white Gaussian noise.



Fig. 1. Diagram of a 2×2 MIMO system with a ZF receiver and two equal-power data streams.

of the power corresponding to each of the two streams by decoupling the 2×2 MIMO channel matrix. Depending on the availability of the channel state information (CSI), the MIMO decoupling can take different forms. Provided the CSI is known at both transmitter and receiver sides, the MIMO channel decoupling can be easily done via singular value decomposition (i.e., by beamforming each of the data streams to a distinct eigenmode of the MIMO channel) [9]. In practice, the receiver can learn the channel e.g., via a training sequence. However, due to finite coherence time of the fading channel and the feedback overhead, CSI is often unknown to the transmitter. In this case, the MIMO channel decoupling can be achieved at the expense of a higher complexity at the receiver. In this work, we assume a zero-forcing (ZF) receiver [9] and a transmitter with full spatial multiplexing (see Fig. 1), which is in agreement with the open-loop configuration of the measurement.

For each OFDM subcarrier (i.e., a frequency tone corresponding to the discrete Fourier transform of the OFDM symbol), the MIMO channel is assumed to be flat,² i.e.,

$$\mathbf{y} = \mathbf{H}\mathbf{x} + \mathbf{n} \quad (3)$$

where \mathbf{H} is the MIMO channel at the subcarrier frequency, \mathbf{x} and \mathbf{y} are the transmitted and received signal vectors, respectively, and \mathbf{n} is the noise vector with independent identically distributed (i.i.d.) unit variance Gaussian elements. Note that we for notational convenience do not use any index for the subcarrier in the flat channel model (3). Let now \mathbf{h}_i be the i th column of \mathbf{H} and x_i be the i th element of \mathbf{x} , where $i = 1, \dots, N_t$ (with the number of transmit antennas denoted as N_t). Then, (3) can be rewritten as

$$\mathbf{y} = \mathbf{h}_i x_i + \sum_{j \neq i} \mathbf{h}_j x_j + \mathbf{n}. \quad (4)$$

The first term in the right side of (4) corresponds to the i th (intended) stream, and the second term represents the interference with respect to the i th stream caused by all the other streams. A ZF receiver projects the i th stream into the subspace orthogonal to the one spanned by $\mathbf{h}_1, \dots, \mathbf{h}_{i-1}, \mathbf{h}_{i+1}, \dots, \mathbf{h}_{N_t}$. Then, also following [9], the power (that is equal in value to the signal-to-noise ratio due to the unit variance noise assumption) of the i th stream becomes

$$P_i = \frac{1}{[(\mathbf{H}^H \mathbf{H})^{-1}]_{i,i}} \quad (5)$$

where the superscript H stands for conjugate transpose, and $[\mathbf{X}]_{i,i}$ denotes the i th diagonal entry of the matrix \mathbf{X} . By now, we can use (5) to decouple the MIMO channel and to calculate the power corresponding to each stream.

Note that we assumed a flat channel (3) over each OFDM subcarrier. Therefore, we adopt the same method as in [6] in order to take into account the OFDM effect: We coherently combine the different independent subcarriers and divide the power by the number of independent subcarriers.

²A flat channel means that the channel stay constant in the frequency domain, i.e., the coherence bandwidth of the channel is much larger than the subcarrier bandwidth.

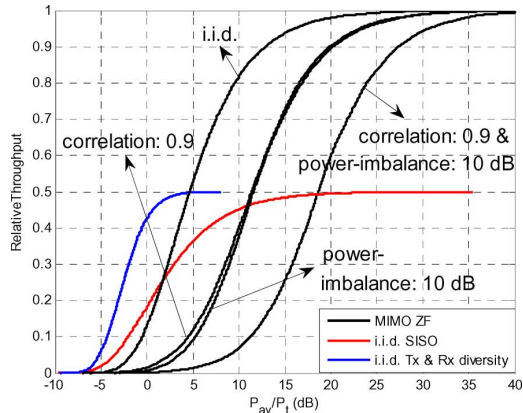


Fig. 2. Relative throughput of a 2×2 MIMO system (denoted as ZF and shown as black curves) with ideal antennas, a complex amplitude correlation magnitude of 0.9 but no power-imbalance, a complex amplitude correlation magnitude of 0.9 but a 10-dB power-imbalance, and a correlation of 0.9 and a 10-dB power-imbalance. For comparison, the throughputs of an i.i.d. SISO channel and an i.i.d. MIMO channel with 4-order spatial diversity but no multiplexing (denoted as i.i.d. Tx & Rx diversity) are also plotted in the same figure.

III. SIMULATION

Using the MIMO throughput model developed in the previous section, we can study the MIMO antenna effects (i.e., correlation and power imbalance) on the throughput in a RIMP environment. For simplicity we focus on the receive antenna effect in this communication. The MIMO channel including the overall antenna effect can be expressed as [12]

$$\mathbf{H} = \mathbf{R}^{1/2} \mathbf{H}_w \quad (6)$$

where \mathbf{H}_w denotes the spatially white MIMO channel with i.i.d. complex Gaussian elements, $\mathbf{R}^{1/2}$ is the Hermitian square root of \mathbf{R} , which is

$$\mathbf{R} = \mathbf{\Xi} \circ \mathbf{\Phi} \quad (7)$$

where $\mathbf{\Xi} = \sqrt{\mathbf{e}} \mathbf{e}^T$ with \mathbf{e} denoting a vector consisting the embedded radiation efficiencies at each port of the MIMO antenna, the superscript T is the transpose operator, $\sqrt{\cdot}$ is the element-wise (i.e., the operation is performed on each of the elements) square root, \circ denotes element-wise product, and the correlation matrix $\mathbf{\Phi}$ consists of the complex correlation coefficients at the MIMO antenna.

For the simulation, we assume a 2×2 MIMO system as in the measured case, where the transmit antennas are ideal (in the sense that they have unity embedded radiation efficiency and no correlation) and the receive antennas have different embedded radiation efficiencies and nonzero correlation.

We generate a 2×2 i.i.d. Gaussian matrix with 100000 realizations and introduce power imbalance and correlation to the MIMO channel via (6). We apply ZF equalization at the receiver to decouple the channel, and determine the CDFs and thereafter the throughput using (2). The calculated MIMO throughputs for some different MIMO antenna cases are shown in Fig. 2. For comparison, an i.i.d. SISO channel and an i.i.d. MIMO channel with 4-order spatial diversity but no multiplexing gain (denoted as i.i.d. Tx & Rx diversity) are also shown, respectively. The four multiplexing throughput curves (black) show the effect of both correlation and power-imbalance between the receive antenna ports.

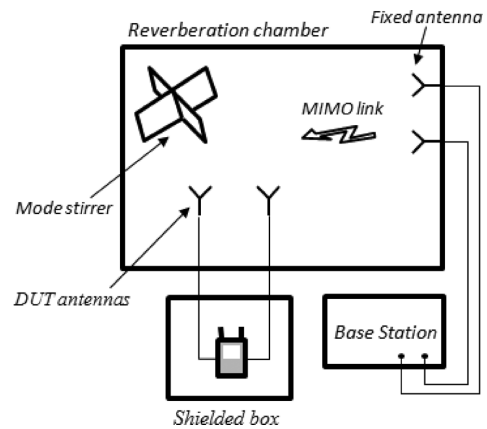


Fig. 3. Measurement setup for 2×2 MIMO LTE throughput tests.

IV. MEASUREMENT

The throughput measurement setup is shown in Fig. 3. We used the Bluetest RTS60 RC for the measurement. Note that the actual mode stirrers used are two metal plates (moving along two different walls inside the RC) with sizes of $97 \times 40 \text{ cm}^2$ and $88 \times 30 \text{ cm}^2$, respectively (see [13, Sec. II]). A commercial communication test instrument with spatial multiplexing capability was used as the base station. The MIMO receiver under test is a commercial LTE USB dongle with external radio frequency (RF) ports for OTA tests. The USB dongle was located in a separate shielded box outside the RC. It is connected with two discone antennas (via RF cables) that are located inside the RC. The measurements were conducted for downlink communications in an open loop configuration (i.e., the base station has no CSI).

The two discone antennas were orthogonally placed with sufficient separation in the chamber, so that the antennas are uncorrelated. We performed measurements for several power imbalances by introducing different attenuators on one of the antenna ports. The dongle's built-in antennas are not connected once the external RF ports are used. In order to create the random fading environment, the mode stirrers (see e.g., [13]) were continuously moving during the measurement. It is known that the Doppler spread affects the orthogonality of the OFDM subcarrier channels, and therefore degrades the throughput. Due to mechanical reasons, the stirring speed in the used RC is limited to 0.2 m/s. This stirring speed results in a negligible Doppler spread, and therefore little effects on the measured throughput. As a result, the measurements correspond to slow fading (e.g., indoor) environments. It is also known that the coherence bandwidth directly affects the number of independent OFDM subcarrier channels. A smaller coherence bandwidth results in a steeper slope of the measured throughput (up to a limit where delay spread equals the length of the cyclic prefix of the OFDM symbols [9]). During the measurement, the RC was loaded to achieve a RMS delay spread of 90 ns (corresponding to 3-MHz coherence bandwidth) [14], [15]. This specific loading was chosen because it is close to that of a typical indoor environment [1] (where 80-ns delay spread was chosen). Measurements were performed on the LTE band 7, i.e., channel 3100 (2655 MHz), with a bandwidth of 10 MHz. The OTA testing system was set to a fixed modulation of 64 QAM with a maximum rate of 40 Mbps. The OFDM partitions the wideband channel into subcarrier channels, some of which may fade independently depending on the coherence bandwidth of the channel. The number of independent subcarrier channels can be approximated by dividing the system bandwidth (10 MHz) by the coherence bandwidth (3 MHz). However, it can be seen from the definition of the coherence bandwidth, e.g., [14], that two subchannels with a separation larger (but not much larger) than 3 MHz still may have a nonzero correlation. Thus the actual number

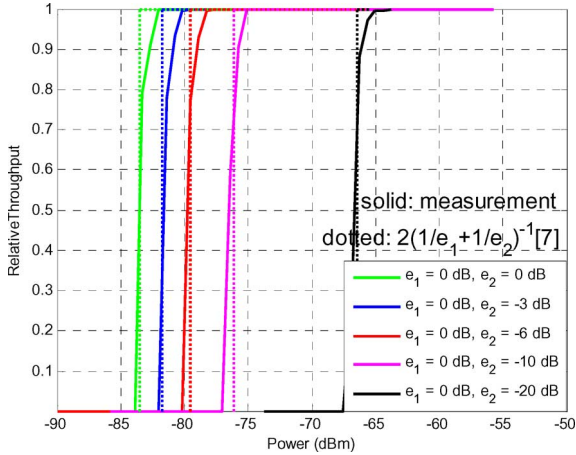


Fig. 4. Relative throughput for conductive measurements (i.e., in an AWGN channel).

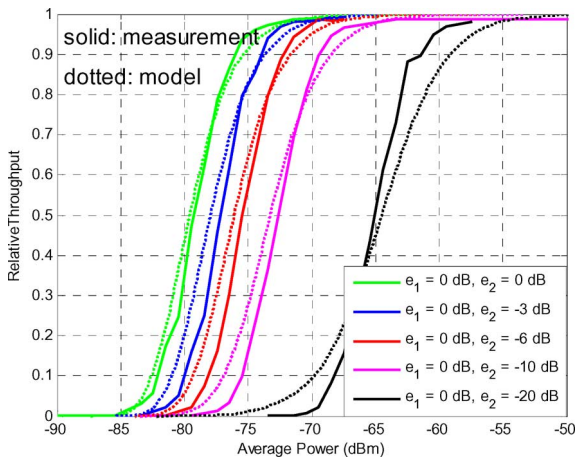


Fig. 5. Relative throughput measurements with continuous mode-stirring in the RC (i.e., in a RIMP environment).

of independent subcarrier channels (or the frequency diversity order) will be smaller. It is shown in [6] for the same RC loading that 2-order frequency diversity is sufficiently to model the OFDM for this measurement setup.

To study the power imbalance effect on the MIMO throughput, the same measurement procedure is repeated with the receive antennas connected with different attenuators. Fig. 4 shows the throughputs in conductive setting (i.e., the transmitter and receiver are connected via RF cables, obtaining an AWGN channel) for different antenna attenuations (i.e., 3 dB, 6 dB, 10 dB, and 20 dB). We see that there are clear threshold transitions in the throughput measurements (cf. Section II). These conductive measurements further validate the threshold receiver model (1). Fig. 5 shows the relative throughputs for the same set of attenuations when measured in the RC with moving stirrers and modeled using the presented throughput model. Note that in both Figs. 4 and 5, $e_i = 0$ dB means that the corresponding antenna is without any attenuator, $e_i = -10$ dB means that the corresponding antenna is connected to a 10 dB attenuator, etc. Also note that the throughputs in both Figs. 4 and 5 are normalized to the sum of the maximum throughputs of both streams (i.e., 24 Mbps). It can be seen from Fig. 5 that the proposed MIMO throughput model can be used to predict the measurement well and that a power imbalance results in a degradation, which we refer to as a spatial multiplexing efficiency. The latter observation is rather intuitive. In order to achieve the spatial multiplexing, the receiver needs

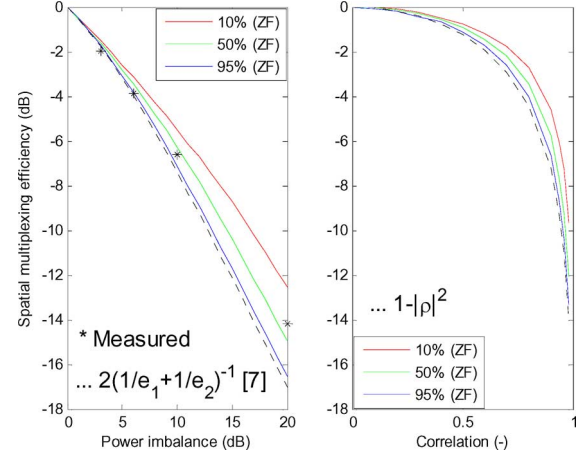


Fig. 6. Throughput multiplexing efficiencies of a 2×2 MIMO system with OFDM and ZF receiver at 10%, 50%, and 95% threshold levels, respectively (see solid curves). The dotted curve is an approximating multiplexing efficiency due to power imbalance [7] and correlation ρ . The measured ones are shown as * for 3-, 6-, 10-, and 20-dB power imbalances. Note that since the measured multiplexing efficiency is about the same at all the threshold levels (see Fig. 4) the measured ones are averaged over the three threshold levels.

to detect both streams; and the detection threshold relies on the branch that has the lower receive power.

The effects of correlation and power imbalance are also shown separately in the two graphs in Fig. 6 as a throughput *multiplexing efficiency* [16], i.e., the degradation compared to the throughput with the same power level on both ports and no correlation between them. We see that a correlation coefficient of 0.9 has almost the same effect on the multiplexing efficiency as a port imbalance of 10 dB. In addition to the simulated multiplexing efficiency as a function of power imbalance and correlation, respectively, the corresponding approximated multiplexing efficiencies, $2e_1e_2/(e_1 + e_2)$ and $1 - |\rho|^2$, are also plotted in the same figure. It shows that the approximated multiplexing efficiencies agree well for the simulated ones at a high throughput level.

V. CONCLUSION

We have extended the SIMO throughput model presented in [6] to the MIMO case with spatial multiplexing. A simple ZF receiver has been implemented in the model and turns out to explain the measured throughput performance very well. The ZF receiver has the smallest spatial diversity among all the open loop MIMO receivers [9]. As a result, we observe that the modeled throughputs have smaller slope than the measured ones, meaning that a more advanced receiver is probably implemented in the USB dongle under test. Nevertheless, there are still reasonable agreements between the modeled and measured throughputs. In addition, using the presented throughput model, we have studied the effects of power imbalance and correlation on the throughput. These are characterized in terms of a spatial multiplexing efficiency, showing 7-dB degradation for a power imbalance of 10 dB and a correlation magnitude of 0.9 at the 95% throughput level, respectively. The effects of power imbalance and correlations seem to be independent, so that the combined effect of 10-dB power imbalance and a 0.9 correlation is a multiplexing efficiency reduction of 14 dB at the same throughput level. The intuitive explanation is that in order to achieve full spatial multiplexing the receiver needs to receive more power so that all the streams can be detected by the threshold receiver. We have shown that throughput measurements in a RIMP environment are useful to quantify the performances of MIMO antenna as well as implemented signal-processing algorithms in the device under test.

REFERENCES

- [1] E. Genender, C. L. Holloway, K. A. Remley, J. M. Ladbury, G. Koepke, and H. Garbe, "Simulating the multipath channel with a reverberation chamber: Application to bit error rate measurements," *IEEE Trans. Electromagn. Compat.*, vol. 52, pp. 766–777, 2010.
- [2] G. Ferrara, M. Migliaccio, and A. Sorrentino, "Characterization of GSM non-line-of-sight propagation channels generated in a reverberating chamber by using bit error rates," *IEEE Trans. Electromagn. Compat.*, vol. 49, no. 3, pp. 467–473, Aug. 2007.
- [3] C. Orlenius, P.-S. Kildal, and G. Poilasne, "Measurement of total isotropic sensitivity and average fading sensitivity of CDMA phones in reverberation chamber," presented at the IEEE AP-S Int. Symp., Washington, DC, USA, Jul. 3–8, 2005.
- [4] N. Arsalane, M. Mouhamadou, C. Decroze, D. Carsenat, M. A. Garcia-Fernandez, and T. Monediere, "3GPP channel model emulation with analysis of MIMO-LTE performances in reverberation chamber," *Int. J. Antennas Propag.*, vol. 2012, no. Article ID 239420, p. 8, 2012.
- [5] R. Recanatini, F. Moglie, and V. M. Primiani, "Performance and immunity evaluation of complete WLAN systems in a large reverberation chamber," *IEEE Trans. Electromagn. Compat.*, no. DOI: 10.1109/TEM.2013.2239636, to be published.
- [6] P.-S. Kildal, A. Hussain, X. Chen, C. Orlenius, A. Skårbratt, J. Åsberg, T. Svensson, and T. Eriksson, "Threshold receiver model for throughput of wireless devices with MIMO and frequency diversity measured in reverberation chamber," *IEEE Antennas Wireless Propag. Lett.*, vol. 10, pp. 1201–1204, 2011.
- [7] P.-S. Kildal, A. Hussain, G. Durisi, C. Orlenius, and A. Skårbratt, "LTE MIMO multiplexing performance measured in reverberation chamber and accurate simple theory," presented at the 6th Eur. Conf. on Antennas and Propagation (EUCAP), Prague, Czech, Mar. 26–30, 2012.
- [8] P.-S. Kildal, C. Orlenius, and J. Carlsson, "OTA testing in multipath of antennas and wireless devices with MIMO and OFDM," *Proc. IEEE*, vol. 100, no. 7, pp. 2145–2157, Jul. 2012.
- [9] A. Paulraj, R. Nabar, and D. Gore, *Introduction to Space-Time Wireless Communication*. Cambridge, U.K.: Cambridge Univ. Press, 2003.
- [10] Z. Kang, K. Yao, and F. Lorenzelli, "Nakagami-m fading modeling in the frequency domain for OFDM system analysis," *IEEE Commun. Lett.*, vol. 7, no. 10, pp. 484–486, Oct. 2003.
- [11] N. Prasad and M. K. Varanasi, "Outage theorems for MIMO block-fading channels," *IEEE Trans. Inf. Theory*, vol. 58, no. 7, pp. 2159–2168, Jul. 2006.
- [12] X. Chen, P.-S. Kildal, J. Carlsson, and J. Yang, "MRC diversity and MIMO capacity evaluations of multi-port antennas using reverberation chamber and anechoic chamber," *IEEE Trans. Antennas Propag.*, vol. 61, no. 2, pp. 917–926, Feb. 2013.
- [13] P.-S. Kildal, X. Chen, C. Orlenius, M. Franzén, and C. Lötbäck Patané, "Characterization of reverberation chambers for OTA measurements of wireless devices: Physical formulations of channel matrix and new uncertainty formula," *IEEE Trans. Antennas Propag.*, vol. 60, no. 8, pp. 3875–3891, Aug. 2012.
- [14] X. Chen and P.-S. Kildal, "Theoretical derivation and measurements of the relationship between coherence bandwidth and RMS delay spread in reverberation chamber," presented at the 3rd Eur. Conf. on Antenna and Propagation (EuCAP), Mar. 23–27, 2009.
- [15] O. Delangre, P. D. Doncker, M. Lienard, and P. Degauque, "Delay spread and coherence bandwidth in reverberation chamber," *Electron. Lett.*, vol. 44, no. 5, Feb. 2008.
- [16] R. Tian, B. K. Lau, and Z. Ying, "Multiplexing efficiency of MIMO antennas," *IEEE Antennas Wireless Propag. Lett.*, vol. 10, pp. 183–186, 2011.